SAFE STAB 2021
Stability and Safety of Ships and Ocean Vehicles

Proceedings of the 1st International Conference on the Stability and Safety of Ships and Ocean Vehicles, 7-11 June 2021, Glasgow, Scotland, UK

Time-domain simulation of the manoeuvring performance of ships in regular waves and shallow water

Christos Pollalis, *Maritime Risk Group, National Technical University of Athens*,

cpol@mail.ntua.gr

Evangelos Boulougouris, *Maritime Safety Research Centre, University of Strathclyde*,

evangelos.boulougouris@strath.ac.uk

ABSTRACT

The IMO's Second Generation of Intact Stability Criteria (SGISC) have brought the manoeuvring performance of ships in waves to the spotlight of the research community. A very interesting case arises when the vessel's manoeuvrability is affected by shallow water as well. As this instance is rather common closer to shore and in the proximity of ports, any degradation of the vessel's ability to execute the commanded manoeuvres may give rise to safety concerns. The authors present herein a novel hybrid methodology that captures such changes in the ship's manoeuvring performance. It accounts for the influence of both the first and second-order wave forces, as well as on the calm water-related contributions. This hybrid seakeeping and manoeuvring methodology has been programmed into the time-domain simulation software ELIGMOS and it is tested with the S-175 container ship, investigating the impact on her turning circle manoeuvres in long regular waves ($\lambda/L=1.0$) at a Froude number of 0.15 and various under keel clearance values. The steady drift forces in shallow water have been calculated using a near-field methodology, embedded in the NEWDRIFT 3D-panel code. Using Ankudinov's formulae, the impact of shallow water on the manoeuvring derivatives has been captured. The authors present analytically the results and discuss their findings.

Keywords: shallow-water waves, manoeuvring in waves, time-domain simulation, turning ability

1. INTRODUCTION

The manoeuvring performance of a marine vessel in waves has been a field of extensive research for more than 40 years implementing experimental (e.g. Moctar et al., 2016) with several numerical methods proposed by scholars. The introduction of the EEDI (MEPC.212(63)) (IMO 2012) aimed at achieving more environmentally efficient design and operation of new ships. However, serious concerns have been raised regarding the minimum powering and steering capabilities that ensure their safe navigation, especially when manoeuvring to avoid

collision with other ships or other surroundings in adverse weather conditions. The aforementioned were addressed within the EU funded RTD project SHOPERA (www.shopera.org), where in-depth research, valuable assessment framework and evaluation methods concerning a marine vessel's manoeuvrability in extreme environmental conditions have been introduced (MEPC 70-INF.33). Furthermore, IMO's Second Generation Intact Stability Criteria (SGISC) have underlined the need for a better understanding of the stability of a ship in waves, incorporating manoeuvring related forcing. This is an explicit requirement in MSC.1/Circ.1627 (IMO, 2020) for capturing non-linear phenomena such as broaching-to and parametric rolling failure modes. SGISC have also paved the way for applying numerical simulation tools for the direct assessment of intact stability (Level 3 approach).

Concerning the methodologies implemented within the numerical simulation domain, they can be grouped in two categories: The first one, or the so-called hybrid (e.g. Bailey et al., 1998), blends the effects of the calm water manoeuvring and seakeeping contributions in a common set of equations. The other, is formulated in a two-time scaling approach (Skejic & Faltinsen, 2008). It distinguishes the manoeuvring and the seakeeping modules which are solved independently and interact at certain time steps through the vessel's instantaneous longitudinal speed and heading angle.

The majority of the conducted studies investigate the manoeuvring performance of marine vessels in regular waves, whilst some others (e.g. Hasnan & Yasukawa, 2020) provide novel approaches that allow the calculation of the first and mean second-order wave forces.

Recently, the 29th ITTC Specialist Committee on Manoeuvring in Waveshighlighted the need to extend the scientific efforts towards the incorporation of the shallow water effects as well (ITTC, 2021). Such conditions appear mainly when large ships sailing close to the shore or harbour areas where the under keel clearance is reduced. Simultaneously at these areas the collision risk with other ships is higher due to the denser marine traffic.

In Ruiz et al. (2019) the combined impact of shallow water conditions together with regular waves on the turning ability of an Ultra Large Container Ship (ULCS) have been investigated. The authors implemented the two-time scale approach. Experiments were carried out as well, showing that the oscillatory environment induced by the waves does not influence the propeller's and the rudder's actions.

In the context of the present study, an empirical formulation is proposed that can be used for simulating the turning motion of a ship in regular waves and shallow water. This is conducted for 4 values of under keel clearance, namely h/d=3.0, 2.5, 2.0 and 1.5, through a hybrid numerical simulation code (ELIGMOS) where calm water manoeuvring

and seakeeping-related external forces are added up at each time step. Calm water manoeuvring terms follow the MMG approach, whereas the wave forces are imported adopting a multidimensional interpolation scheme based on the vessel's instantaneous longitudinal speed and heading angle. Additionally, the effect of shallow water is considered at each force component by adopting regression formulae according to Furukawa et al. (2016), Ankudinov et al. (1990), Amin and Hasegawa (2010) (calm water resistance, lift-drag viscous forces, hull-propeller-rudder interaction coefficients) and the 3D panel code NEWDRIFT v.7. Simulations are performed considering small wave amplitude (H=2m) and long wavelength (λ/L=1.0, 1.2). The results are presented and discussed in order to extract qualitative conclusions rather than quantitative, due to the lack of directly comparable experimental data.

2. METHODOLOGY

In this section, a presentation of the developed methodology is provided, starting from the definition of the coordinate systems and governing equations. Subsequently, details on the methods adopted for the calculation of each force component are given as well.

2.1 Coordinate systems

Two coordinate systems are used in the context of the present numerical approach. As it is depicted in Fig. 1, the first oneis the earth-fixed OXYZ and the second is a slowly varying body-fixed oxyz that follows the vessel's trajectory during turning.

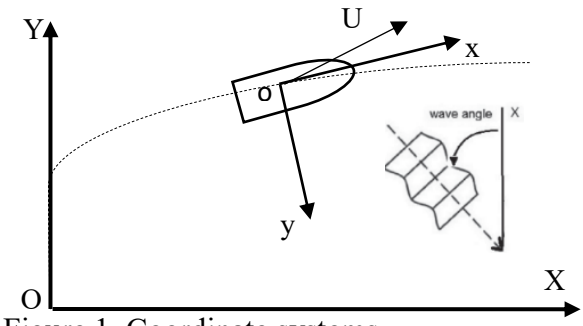

Figure 1. Coordinate systems

Surge and sway velocities are transformed from the body-fixed system (u, v) to the earth-fixed (U, V), using the following equations:

$$\begin{cases} U = \cos\psi \cdot u - \sin\psi \cdot v \\ V = \sin\psi \cdot u + \cos\psi v \end{cases} \quad (1)$$

In Eq. (1) ψ stands for the instantaneous yaw angle.

2.2 Mathematical modelling

The numerical approach presensented herein considers the ship's turning motion on the horizontal plane thus, a 3DOF system of equations is employed with respect to surge, sway and yaw motions as shown in Eqs. 2, 3 and 4. The vessel's vertical motions are out of scope as phenomena like squat in shallow water will be investigated in the future.

$$\text{Surge: } (M + M_x)\ddot{u} = X_{FK} + X_{DIFF} + X_{AR} + X_{HD} + X_R + (1 - t)T - R \quad (2)$$

Sway: $(M + M_y)\ddot{v} + Mx_G\ddot{r} = Y_{FK} + Y_{DIFF} + Y_{HD} + Y_{DF} + Y_R$ (3)

Yaw: $(I_{zz} + J_{zz})\ddot{r} + Mx_G\ddot{v} = N_{FK} + N_{DIFF} + N_{HD} + N_{DF} + N_R$ (4)

In Eqs. (2), (3) and (4) u, v, r refer to surge,-sway and yaw velocities expressed at the body-fixed reference frame and the subscripts FK, DIFF, HD, T, R denote the Froude-Krylov, diffraction, hydrodynamic hull forces, thrust and rudder forces respectively. Subscripts AR, DF indicate the steady added resistance and sway and yaw drift forces. The variables M, I_{zz} stand for the ship's mass and moment of inertia about her vertical axis. M_x, M_y, and J_{zz} are the added masses and added moment of inertia with respect to the vessel's body-fixed axes respectively.

Subsequently, a detailed presentation of the calculation process for each force component is provided.

2.3 Wave forces

As mentioned before, first and second-order wave forces for the S-175 container ship (Fig. 2) have been calculated assuming potential flow characteristics using the hydrodynamic software NEWDRIFT v.7. The aforementioned software adopts a 3D panel method, where the velocity potential Φ is decomposed into a steady (S) and a time-dependent (T) part as indicated below.

$$\Phi(x, y, z; t) = -Ux + \Phi_S(x, y, z) + \Phi_T e^{-i\omega t} \quad (5)$$

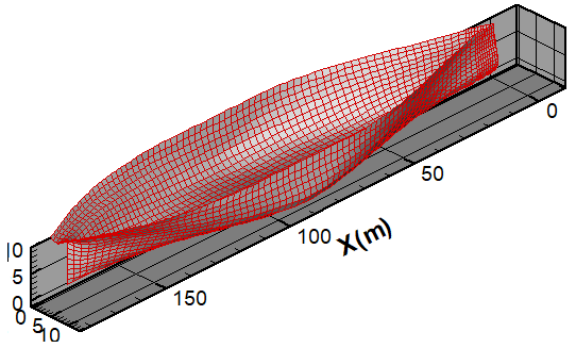

Figure 2. Panel geometry of S-175 (T=9.5m)

Decomposing further the unsteady potential Φ_T leads to the formulation of Eq. 6, where the quantities at the RHS refer to the incident (I), the diffracted (D) and the radiation potentials (R).

$$\Phi_T = \Phi_I + \Phi_D + \sum_{j=1}^{6} \xi_j \Phi_{R,j} \quad (6)$$

In Eq. 6 the incident potential is expressed according to the following expression (Papanikolaou, 1985):

$$\varphi_I = \frac{1}{k}\frac{\cosh k_0(z+h)}{\cosh k_0 h} e^{ik_0(x\cos\chi + y\sin\chi)} \quad (7)$$

In the previous expression, h is the sea depth and χ is the wave's heading angle. Additionally, k is the frequency number that can be determined through the dispersion relationship (Eq. 8).

$$k = k_0 \tanh k_0 h \quad (8)$$

The velocity potentials Φ_j (j=0, 1, 2…,7) must satisfy the following boundary conditions in the fluid domain, the free surface and the sea bed:

$$\begin{cases} \nabla^2\varphi_i = 0, \text{Laplace equation} \\ -\omega^2\varphi_\iota + g\frac{\partial\varphi_i}{\partial z} = 0, \text{linearised free surface condition} \\ \frac{\partial\varphi_i}{\partial z} = 0, \text{on the sea bed } z = -h \end{cases} \quad (9)$$

Additionally, the body boundary condition must be satisfied on the vessel's hull as it is determined below;

$$\frac{\partial\varphi_i}{\partial\vec{n}} = n_i \quad (10)$$

$$\frac{\partial\varphi_D}{\partial\vec{n}} = -\frac{\partial\varphi_i}{\partial\vec{n}} \quad (11)$$

In Eqs. (10) and (11) n stands for the surface normal vector.

In order to incorporate the first-order wave forces into the time-domain software, the following expression is adopted (Fonseca and Soares, 1998).

$$F(t) = Re\{(F_I(u,\chi) + F_D(u,\chi))e^{i\omega_e t}\} \quad (12)$$

The values of the Froude-Krylov and diffraction forces are selected among a number of precalculated values using a multidimensional interpolation scheme which is a function of the instantaneous longitudinal speed and heading angle. Details on the aforementioned scheme are given later in subsection 2.3.1.

The mean second-order wave forces for the considered ship motion on the horizontal plane consist of the added resistance, the sway and yaw drift forces. Therefore, they are important for capturing the physics of the problem. Since long wavelength is considered within the performed simulations, the aforementioned forces have been determined for a number of forward speeds and heading angles using NEWDRIFT v.7 which implements a near-field method (Papanikolaou and Zaraphonitis, 1987) performing direct pressure integration over the wetted surface of the vessel.

2.3.1 Multidimensional interpolation scheme

As mentioned earlier, first and second-order wave forces have been precalculated for several forward speeds and heading angles. More specifically, these involve 4 speeds (Fn=0, 0.05, 0.10 and 0.15) and 19 heading values (χ=0° to 180° with an increment of 10°). Afterwards, a practical scheme is employed in order to incorporate the aforementioned forces during numerical simulations. This concerns General Newton's Interpolation Rule (Dahlquist and, 2003). According to this method, given the instantaneous heading of the vessel (χ_{inst}), the values of each first and second-order wave force with respect to the 4 different forward speeds are determined, i.e. $F_1(\chi_{inst.})$, $F_2(\chi_{inst})$. $F_3(\chi_{inst})$ and $F_4(\chi_{inst})$ implementing linear interpolation. Then, the final interpolated value with respect to the exact forward speed value is determined using the following expressions:

$$\mu_1 = \frac{F_2(\chi_{inst}) - F_1(\chi_{inst})}{u_2 - u_1} \quad (13)$$

$$\mu_2 = \frac{F_3(\chi_{inst}) - 2\cdot F_2(\chi_{inst}) + F_1(\chi_{inst})}{(u_2 - u_1)(u_3 - u_1)} \quad (14)$$

$$\mu_3 = \frac{F_4(\chi_{inst}) - 3 \cdot F_3(\chi_{inst}) + 3 \cdot F_2(\chi_{inst}) - F_1(\chi_{inst})}{(u_2 - u_1)(u_3 - u_1)(u_4 - u_1)} \quad (15)$$

To enhance the accuracy of the interpolation scheme, a varying amount of spline generated values has been utilised.

2.4 Calm water manoeuvring forces

Calm water manoeuvring forces have been calculated according to the Japanese MMG proposed methodology. In this respect, the various force components are calculated in a modular form. Subsequently, the various modules will be presented together with the applied empirical corrections concerning the shallow water effect.

2.4.1 Hydrodynamic (hull) forces

Sway and yaw hydrodynamic lift, drag and cross-flow force components have been evaluated through a third-order nonlinear representation in order to comply with Ankudinov et al's. proposed regression formulae:

$$Y'_H = Y'_v v' + Y'_r r' + Y'_{v|v|} v'|v'| + \\ + Y'_{vrr} v' r'^2 + Y'_{r|r|} r'|r'| \quad (16)$$

$$N'_H = N'_v v' + N'_r r' + N'_{v|v|} v'|v'| + \\ + N'_{vrr} v' r'^2 + N'_{r|r|} r'|r'| \quad (17)$$

Surge hydrodynamic forces consist of the following components:

$$X'_H = X'_0 + X'_{vv} v'^2 + X'_{vr} v' r' + X'_{rr} r'^2 \quad (18)$$

In Eqs. (15)-(18) v', r' denote the nondimensional sway velocity and yaw rate, whereas the deepwater values of the manoeuvring derivatives have been determined from CMT tests. Additionally, X'_0 is the nondimensional calm water resistance coefficient which was also determined through relevant experiments. Furukawa et al. (2016) proposed the following expression in order to account for the shallow water effect:

$$\frac{[X'_0]_{shallow}}{[X'_0]_{deep}} = 0.388 \left(\frac{T}{h}\right)^2 \quad (19)$$

The finite depth sway and yaw added inertia coefficients $X_{\dot{u}}$, $Y_{\dot{v}}$ and $N_{\dot{r}}$ have been calculated implementing Li and Wu's (1990) regression formulae.

2.4.2 Propeller force

The MMG method suggests the following expression for the calculation of the vessel's thrust force:

$$T = (1 - t_p) \rho n_p^2 D_p^4 K_T(J_p) \quad (20)$$

In Eq. (20) t_p is the thrust deduction coefficients, n_p the propeller's revolutions, D_P the propeller's diameter and $K_T(J_P)$ the thrust coefficient. The propeller's advance coefficient J_P is determined using the following expression:

$$J_p = \frac{u(1 - w_p)}{n_p D_p} \quad (21)$$

In Eq. (21) w_P is the vessel's wake fraction at zero drift angle. An expression has been proposed by Amin and Hasegawa for its consideration at finite depth conditions. They have also suggested a regression formula that evaluates the small changes in t_p in finite depth.

2.4.3 Rudder force

Rudder forces in the surge (X_R), sway (Y_R) and yaw (N_R) directions have been calculated according to the following formulae:

$$X_R = -(1 - t_R)FN\sin\delta \quad (24)$$
$$Y_R = -(1 + a_H)FN\cos\delta \quad (25)$$
$$N_R = -(x_R + a_H x_H)FN\cos\delta \quad (26)$$

In the former equations, δ stands for the rudder's angle, x_R is the longitudinal position of the rudder, FN is the normal force applied on the rudder's surface, whilst a_H, x_H and t_R are rudder-hull interaction coefficients.

The normal force FN is calculated using the following expression:

$$FN = \frac{1}{2}\rho A_R f_a U_R^2 \sin a_R \quad (27)$$

In Eq. (27) A_R is the rudder's area, U_R is the rudder's inflow velocity and a_R is the effective inflow angle. Moreover, f_a is the rudder's lift coefficient's gradient. The aforementioned quantities have been calculated using the following formulae:

$$U_R = \sqrt{u_R^2 + v_R^2} \quad (28)$$

$$a_R = \delta - \arctan\left(\frac{v_R}{u_R}\right) \quad (29)$$

In the former expressions u_R, v_R denote the rudder's longitudinal and transverse inflow velocity components which can be determined by adopting the following formulae:

$$u_R = \varepsilon u(1 - w_p) \cdot \cdot \sqrt{\eta\left[1 + \frac{k_x}{\varepsilon}\left(\sqrt{1 + \frac{8K_T}{\pi J_p^2}} - 1\right)\right] + (1 - \eta)} \quad (30)$$

$$v_R = U\gamma_R\beta_R \quad (31)$$

In the last two expressions $\eta=D_p/H_R$ (ratio of propeller diameter over rudder's height), $\varepsilon=(1-w_R)/(1-w_p)$, k_x is the propeller race amplification factor and γ_R is the so-called flow straightening coefficient. In the case of k_x and γ_R, Amin and Hasegawa (2010) propose relevant regression formulae as functions of the under keel clearance and the vessel's principal particulars to account for the finite depth effect.

3. RESULTS AND DISCUSSION

The presented methodology has been implemented through the in-house numerical code ELIGMOS to simulate the port and starboard turning motion of S-175 in regular waves (head and beam) and shallow water. The considered environmental conditions refer to $\lambda/L=1.0$ and $H=2m$, where λ and H correspond to the wavelength and wave height respectively. The ship sails at a Froude number of 0.15, whereas the rudder is

deflected at an angle of ±35°. Additionally, 4 under keel clearance (UKC) values are tested that correspond from medium-deep down to shallow water.

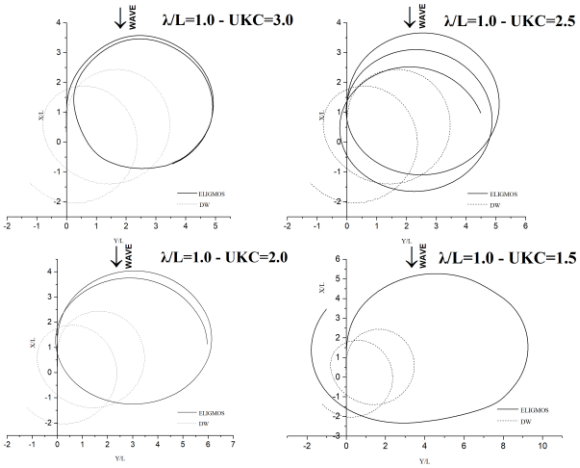

Figure 3. Starboard turning circles of S-175 in regular head waves at different sea depths (λ/L=1.0)

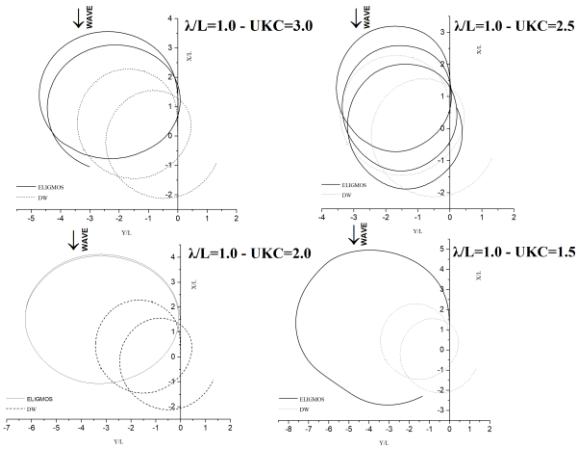

Figure 4. Port turning circles of S-175 in regular head waves at different sea depths (λ/L=1.0)

As it is can be seen from the turning trajectories in regular head waves (Figs. 3, 4), they become larger compared to the deep water condition (DW) as the sea depth reduces with a major impact when UKC=2.0 and 1.5. More specifically, in the case of the starboard turning circle, the advance increases by 1L to 2.5L, whereas the tactical diameter by 1.5L to 5.5L as the UKC decreases. A similar trend is found for the advance's characteristic value in port turning circles, whereas smaller differences are noticed for the tactical diameter. These vary between 1.5L and 4.5L as the UKC reduces. In most cases, a weak influence of the sway drift force is recorded.

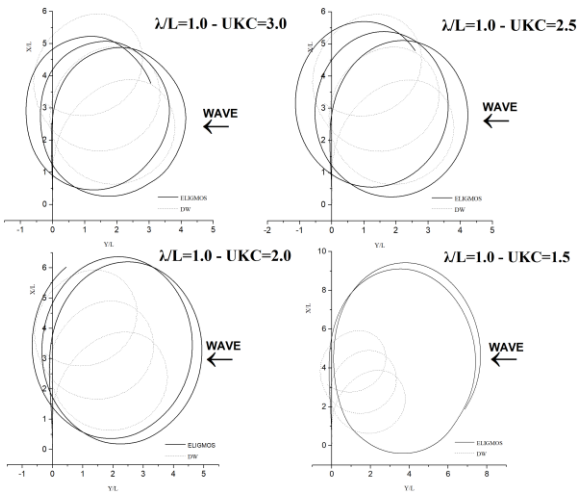

Figure 5. Starboard turning circles of S-175 in regular beam waves at different sea depths (λ/L=1.0)

In the case of starboard turning motion in regular beam waves, it is noticed an increase of the advance varying from 1.5L to 5.5L which is much larger than the relevant case in head waves. This is attributed to the fact that in the latter, the added resistance reduces the forward speed of the vessel resulting in smaller advance values.

On the contrary, the differences in the tactical diameter between the finite depth and deep water cases are found between 0.5L and

4.5L which is smaller than the relevant values in head waves.

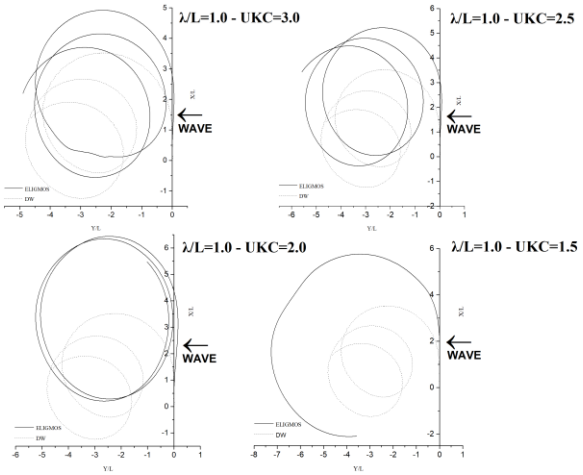

Figure 6. Port turning circles of S-175 in regular beam waves at different sea depths (λ/L=1.0)

This is related to the beam direction of the waves which counteracts the vessel's motion. In the case of port circular motion in beam waves, the advance in finite depth conditions varies from 1.5L to 2.5L compared with the deep water scenario, whereas the tactical diameter is 0.5L to 3.5L larger. This is significantly smaller than the corresponding case in head waves. This time, the wave action seems to contribute to the faster turning of the ship. In both port and starboard turning motion in regular beam waves, it is also encountered a weaker impact of the sway drift force than in the deep water condition.

4. CONCLUSIONS

The present study, presents a methodology for simulating the turning ability of marine vessels in regular waves (head and beam) incorporating 1st as well as 2nd order wave forces and shallow water effects. This has been succeeded using the in-house numerical code ELIGMOS where all the principal external forces have been incorporated, taking into account the finite depth effect. For this purpose, four different UKC values (corresponding to medium deep and shallow water conditions) have been tested to draw preliminary conclusions about the vessel's behaviour, although relevant experimental data that could be used for validation purposes were not available.

In general, the derived trajectories have larger advance and tactical diameter than the deep water scenario, which varied with respect to the initial wave's direction. The weak influence of the sway drift force has been noticed as well. It is suggested that the physics of the problem should be further investigated to extract more robust conclusions. Investigation of the vessel's turning ability at lower forward speed is also suggested, as it consists of a scenario closer to the real operational conditions of large marine vessels when entering a port.

5. REFERENCES

Amin, O., & Hasegawa, K. (2010). 'Generalised Mathematical Model for Ship Manoeuvrability Considering Shallow Water Effect', *Conference Proc. of Japan Society of Naval Architects and Ocean Engineers*.

Ankudinov, V. K., Miller, E. R., Jakobsen, B. K., & Daggett, L. L. (1990). 'Maneuvering performance of tug/barge assemblies in restricted waterways', *Proceedings of*

MARSIM & ICMS 90, Tokyo, Japan.

Bailey, P. A., Price, W. C., Temarel P. (1998). 'A unified mathematical model describing the manoeuvring of a ship travelling in a seaway', *RINA*, vol. 140, pp. 131–149.

EC, Energy Efficient Safe Ship OPERAtion (SHOPERA) (2013-2016), https://cordis.europa.eu/project/id/605221 (accessed on 11 May 2021)

Fonseca, N., & Soares, C. G. (1998). 'Time-domain analysis of large-amplitude vertical ship motions and wave Loads', *Journal of Ship Research, 42*(2), pp. 139-153.

Furukawa, Y., Ibaragi, H., Nakiri, Y., Kijima, K. (2016). 'Shallow Water Effects on Longitudinal Components of Hydrodynamic Derivatives', *4th MASHCON*, Hamburg.

Hansan, M. A., Yasukawa, H. (2020). '6-DOF Motion Simulation of a Ship Turning in Irregular Waves', *33rd Symposium of Naval Hydrodynamics*, Osaka, Japan.

IMO. (2012). 'Guidelines on the method of calculation of the attained energy efficient design index (EEDI) for new ships', *resolution MEPC. 212(63).*

IMO (2020). "Interim Guidelines On The Second Generation Intact Stability Criteria", MSC.1/Circ.1627, 10 December 2020.

ITTC. (2021). 'The Specialist Committee on Manoeuvring in Waves', Virtual.

Li, M., & Wu, X. (1990). 'Simulation calculation and comprehensive assessment on ship maneuverabilities in wind, wave, current and shallow water', *Proceedings of MARSIM and ICSM 90*, 465). Tokyo, Japan.

Moctar, O., Sprenger, F. Schellin, T. E., Papaniklaou, A. (2016). 'Numerical and Experimental Investigations of Ship Manuevers in Waves', *Proc. 35th ASME Int. Conf. on Ocean, Offshore and Arctic Engineering*, Busan, South Korea.

Papanikolaou, A., & Zaraphonitis, G. (1987). 'On an Improved Method for the Evaluation of Second Order Motions and Loads on 3D Floating Bodies in Waves', *Schiffstechnik, 34*, pp. 170-211.

Ruiz, M. T., Mansuy, M., Donatini, L., Villagomez, J., Delefortrie, G., Lataire, E., Vantorre, M. (2019). 'Wave Effects on the Turning Ability of an Ultra Large Container Ship in Shallow Water', *Proc. 38th ASME Int. Conf. on Ocean, Offshore and Arctic Engineering*, Glasgow, Scotland, UK.

Skejic, R., & Faltinsen, O. M. (2008). 'A unified seakeeping and maneuvering analysis of ship in regular waves'. *Journal of Marine Science and Technology*, 13, pp. 371-394.